Analysis and Suppression of Negative-Sequence Current in Single-Channel Operation of Dual Three-Phase PMSM With Zero Angle Displacement

Zekai Lyu, *Member*, *IEEE*, Shuangxia Niu, *Senior Member*, *IEEE*, Haolan Zhan, *Student Member*, *IEEE*, Tao Wang, *Senior Member*, *IEEE*, Lijian Wu, *Senior Member*, *IEEE*, and K. T. Chau, *Fellow*, *IEEE*

***Abstract*—In high-power applications like wind power generation, dual three-phase permanent-magnet synchronous machines (PMSMs) with two power conversion channels grow in popularity owing to decent fault-tolerant capability. This letter focuses on the current control of dual three-phase PMSMs with zero angle displacement, particularly in scenarios where one channel experiences a malfunction. The influence of asymmetric mutual-inductances on negative-sequence current is investigated. Subsequently, a harmonic control method based on non-integer sliding discrete Fourier transform is proposed to suppress the undesired current harmonics. No additional parameter tuning or digital filters are required, which facilitates engineering implementation and integration. Experimental results on a down-scaled drive system validate the effectiveness of the proposed method.**

***Index Terms*—Dual three-phase permanent-magnet synchronous machine (PMSM), negative-sequence current suppression, sliding discrete Fourier transform.**

I. Introduction

MULTIPHASE permanent-magnet synchronous machines (PMSMs) have found extensive application in industrial fields, including electric propulsion and wind power generation owing to high torque density, high power rating, and decent fault-tolerant capability [1], [2]. The dual three-phase (DTP) PMSM is one of the popular multiphase PMSM configurations, as it can utilize commercial three-phase inverters [3], [4], [5]. Notably, harmonic current suppression is vital for DTP PMSMs, drawing extensive attention from both academia and industry.

According to the angle displacement between the two sets of three-phase windings, the DTP machine can be categorized as asymmetric (30° angle displacement) and symmetrical (0° or 60° angle displacement) DTP machine. For the former, the fifth and seventh harmonic components can be decomposed through vector space decomposition (VSD) [6]. Since the conventional proportional-integral (PI) regulator cannot well the harmonic references, several methods were proposed on the basis of VSD scheme to further reduce current harmonics. In [7], the undesired current harmonics were suppressed by using resonant controllers in parallel with PI regulators. However, the parameter tuning of resonant controller is slightly complicated and the interference between the different frequencies needs to be eliminated. In [8], the fifth and seventh harmonic currents were regulated by PI controller based on multiple synchronous reference frames (SRFs). The harmonics can be converted into dc components within corresponding SRFs by corresponding order synchronous coordinate transformation, and then be detected by low-pass filters. Nevertheless, the used digital

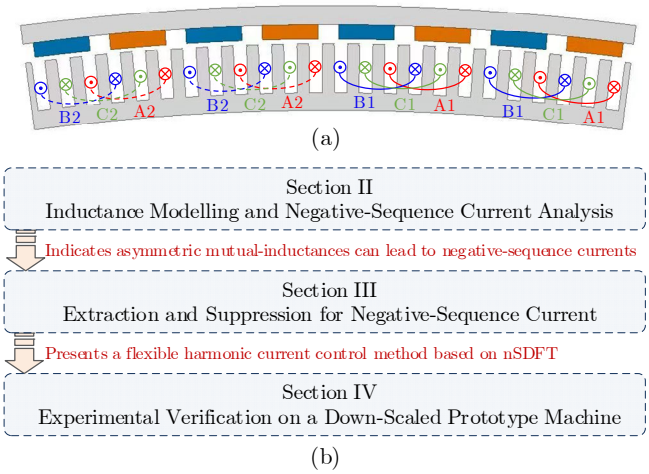

Fig. 1. DTP PMSM with zero angle displacement and associated research contents. (a) Partial model of an external-rotor DTP PM wind power generator. (b) Arrangement of the rest part of this letter.

filters can cause significant delay in the control loop, and careful design of cutoff frequency parameters is crucial for optimal performance. Moreover, the previous researches are mainly focused on asymmetric DTP machines, and the current harmonic issues in symmetrical ones are rarely investigated.

The symmetrical DTP PMSMs, especially those with 0° angle displacement (hereafter referred to as zero angle displacement), can increase the system interchangeability and redundancy. This is achievable because the hardware and software can be identical for controlling both sets of windings. Moreover, DTP PMSMs with zero angle displacement are suitable for modular manufacturing [9]. Hence, this type of PMSM could be a solution for megawatt-level drive systems such as electric ship propulsion and wind turbine generator. For instance, Fig. 1 (a) shows a partial model of a 576-slot/192-pole DTP PM wind power generator with zero angle displacement, which is composed of multiple 24-slot/8-pole base machines and featuring modular stator sectors. Furthermore, it was reported that for 12-slot/10-pole DTP PMSMs, the winding configuration with zero angle displacement can decrease the short-circuit current during fault operations [10]. Noted that for high-power applications like wind power generation, paralleling power conversion channels can be employed to increase the power level and fault-tolerant capability [11]. Specifically, the system can still operate even if the power converter or machine windings of one power conversion line malfunctions. The fault channel can be directly removed, and another set of windings of the DTP machine can operate independently to tolerate faults conveniently. Under this

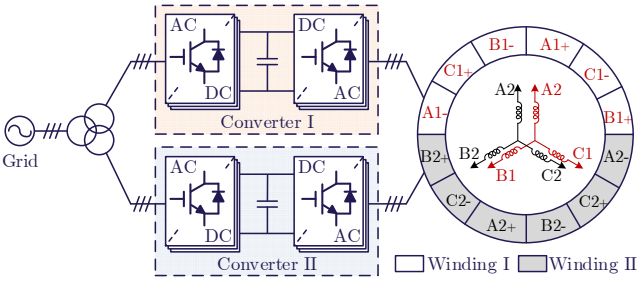

Fig. 2. DTP PMSM drive system with two power conversion channels.

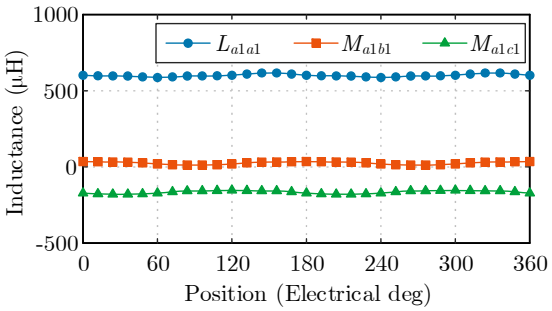

Fig. 3. Inductance waveforms from finite-element analysis.

specific operating condition, additional stator current harmonics may arise. Yet, few studies attempt to carry out in-depth analysis and research on current harmonics in DTP PMSMs with zero angle displacement, especially for conditions where one three-phase channel malfunctions and becomes disconnected.

The rest of this letter follows the structure outlined Fig. 1 (b). This study reveals that in DTP PMSMs with zero angle displacement, asymmetric mutual-inductances can cause the pulsating impedance, which can lead to negative-sequence current when one power channel is cut off. A harmonic control method based on the improved sliding discrete Fourier transform (SDFT) is proposed to suppress the negative-sequence current. Through accurate and real-time sliding spectrum analysis, the control scheme can extract undesired current harmonics and then transform them to corresponding SRFs for regulation. Experimental results are provided to demonstrate the efficacy of the presented analysis and proposed method.

II. Modelling of DTP PMSM With Zero Angle Displacement

Paralleling power conversion lines are commonly used to improve the power level and fault-tolerant capability of large-capacity wind energy conversion systems [11]. The diagram of DTP PMSM drives with two power conversion channels is shown in Fig. 2. In terms of fault-tolerant operation of such multi-unit systems, the most direct approach involves isolating the faulty three-phase set [12]. This method eliminates the need for a custom post-fault algorithm, particularly when each set operates independently regulated, simplifying implementation and enhancing practicality for industrial applications. In the case of DTP PMSM with zero angle displacement, when one three-phase channel malfunctions and is disconnected, the system can operate like a standard three-phase drive system. However, due to the asymmetric relative position within one set of three-phase windings, the mutual inductance between each phase is not the same. This issue is often overlooked, and this Section will provide a detailed analysis.

Ignoring the magnetic saturation, mutual leakage inductance, and core losses, the voltage and flux models in stationary frame can be represented as

$$\begin{cases} \boldsymbol{U}_s = \boldsymbol{R}_s \boldsymbol{I}_s + p\boldsymbol{\psi}_s \\ \boldsymbol{\psi}_s = \boldsymbol{L}_s \boldsymbol{I}_s + \boldsymbol{\psi}_r \end{cases} \tag{1}$$

where p is the derivative operator, $\boldsymbol{U}_s$ is the stator voltage, $\boldsymbol{R}_s$ is the stator resistance, $\boldsymbol{I}_s$ is the stator current, $\boldsymbol{L}_s$ is the winding inductance, $\boldsymbol{\psi}_s$ is the stator flux, and $\boldsymbol{\psi}_r$ is the PM flux. Specifically, $\boldsymbol{L}_s$ can be expressed as

$$\boldsymbol{L}_s = \begin{bmatrix} \boldsymbol{L}_{11} & \boldsymbol{L}_{12} \\ \boldsymbol{L}_{21} & \boldsymbol{L}_{22} \end{bmatrix}_{6*6} \tag{2}$$

where $\boldsymbol{L}_{11}$ and $\boldsymbol{L}_{22}$ represent the inductance matrix of the first and second winding set, respectively, $\boldsymbol{L}_{12}$ and $\boldsymbol{L}_{21}$ represent mutual inductances between two winding sets. All four matrices are 3*3 dimensional matrices, and it is a common practice to assume that $\boldsymbol{L}_{11} = \boldsymbol{L}_{22}$ and $\boldsymbol{L}_{12} = \boldsymbol{L}_{21}$.

Moreover, the inductance waveforms of the machine depicted in Fig. 1 (a), obtained from finite-element analysis, are presented in Fig. 3. The inductance matrix $\boldsymbol{L}_{11}$ at this time can be expressed as

$$\boldsymbol{L}_{11} = \begin{bmatrix} L_{a1a1} & M_{a1b1} & M_{a1c1} \\ M_{b1a1} & L_{b1b1} & M_{b1c1} \\ M_{c1a1} & M_{c1b1} & L_{c1c1} \end{bmatrix} = \begin{bmatrix} L_1 & M_1 & M_2 \\ M_1 & L_1 & M_2 \\ M_2 & M_2 & L_1 \end{bmatrix} \tag{3}$$

where L_{a1a1}, L_{b1b1}, and L_{c1c1} represent self-inductances, M_{a1b1}, M_{a1c1}, M_{b1a1}, M_{b1c1}, M_{c1a1}, and M_{c1b1} represent mutual-inductances, and $M_1 \neq M_2$. This phenomenon is caused by asymmetric relative position within one set of three-phase windings. While the analysis is based on an external-rotor machine, the asymmetric mutual-inductance phenomenon occurs in both external-rotor and internal-rotor machines.

For better representation, the matrix $\boldsymbol{L}_p$ is introduced to represent the inductance matrix of a standard three-phase machine equivalent to two sets of windings connected in parallel [13], which can be expressed as

$$\boldsymbol{L}_p = \begin{bmatrix} L_0 & M_0 & M_0 \\ M_0 & L_0 & M_0 \\ M_0 & M_0 & L_0 \end{bmatrix} \tag{4}$$

Then, (2) can be rewritten as

$$\boldsymbol{L}_s = \begin{bmatrix} \boldsymbol{L}_{11} & \boldsymbol{L}_{12} \\ \boldsymbol{L}_{21} & \boldsymbol{L}_{22} \end{bmatrix}_{6*6} = \begin{bmatrix} \boldsymbol{L}_{11} & 2\boldsymbol{L}_p - \boldsymbol{L}_{11} \\ 2\boldsymbol{L}_p - \boldsymbol{L}_{11} & \boldsymbol{L}_{11} \end{bmatrix}_{6*6}$$

$$= \begin{bmatrix} L_1 & M_1 & M_2 & 2L_0 - L_1 & 2M_0 - M_1 & 2M_0 - M_2 \\ M_1 & L_1 & M_2 & 2M_0 - M_1 & 2L_0 - L_1 & 2M_0 - M_2 \\ M_2 & M_2 & L_1 & 2M_0 - M_2 & 2M_0 - M_2 & 2L_0 - L_1 \\ 2L_0 - L_1 & 2M_0 - M_1 & 2M_0 - M_2 & L_1 & M_1 & M_2 \\ 2M_0 - M_1 & 2L_0 - L_1 & 2M_0 - M_2 & M_1 & L_1 & M_2 \\ 2M_0 - M_2 & 2M_0 - M_2 & 2L_0 - L_1 & M_2 & M_2 & L_1 \end{bmatrix} \tag{5}$$

Using synchronous coordinate transformation, the inductance matrix of one set three-phase winding in SRF can be represented as

$$\boldsymbol{L}_{11dq}=\begin{bmatrix} L_{ave}+\frac{2}{3}M_{asy}\cos\beta & -\frac{2}{3}M_{asy}\sin\beta \\ -\frac{2}{3}M_{asy}\sin\beta & L_{ave}-\frac{2}{3}M_{asy}\cos\beta \end{bmatrix} \tag{6}$$

where L_{ave} represents the average component, M_{asy} represents the asymmetric component of mutual-inductances, and β represents the phase information. They can be expressed as

$$L_{ave}=L_1-\frac{1}{3}M_1-\frac{2}{3}M_2,\quad M_{asy}=M_1-M_2,\quad \beta=2\theta_e-\frac{2}{3}\pi \tag{7}$$

where θ_e is the electrical position. It can be noted that the non-diagonal elements of the inductance matrix in (6) are not zero due to asymmetric mutual-inductances.

Moreover, the voltage equation of one set three-phase winding in the SRF (taking winding I as an example) can be expressed as

$$\begin{aligned}\begin{bmatrix} u_{d1} \\ u_{q1} \end{bmatrix}=&R_s\begin{bmatrix} i_{d1} \\ i_{q1} \end{bmatrix}+\omega_e\begin{bmatrix} \frac{2}{3}M_{asy}\sin\beta & -L_{ave}+\frac{2}{3}M_{asy}\cos\beta \\ L_{ave}+\frac{2}{3}M_{asy}\cos\beta & -\frac{2}{3}M_{asy}\sin\beta \end{bmatrix}\begin{bmatrix} i_{d1} \\ i_{q1} \end{bmatrix}\\ &+\omega_e\begin{bmatrix} -\frac{2}{3}M_{asy}\sin\beta & L_{ave}-\frac{2}{3}M_{asy}\cos\beta \\ -L_{ave}-\frac{2}{3}M_{asy}\cos\beta & \frac{2}{3}M_{asy}\sin\beta \end{bmatrix}\begin{bmatrix} i_{d2} \\ i_{q2} \end{bmatrix}\\ &+2(L_0-M_0)\begin{bmatrix} p & -\omega_e \\ \omega_e & p \end{bmatrix}\begin{bmatrix} i_{d2} \\ i_{q2} \end{bmatrix}+\omega_e\begin{bmatrix} 0 \\ \psi_f \end{bmatrix}\\ &+\begin{bmatrix} L_{ave}+\frac{2}{3}M_{asy}\cos\beta & -\frac{2}{3}M_{asy}\sin\beta \\ -\frac{2}{3}M_{asy}\sin\beta & L_{ave}-\frac{2}{3}M_{asy}\cos\beta \end{bmatrix}p\begin{bmatrix} i_{d1}-i_{d2} \\ i_{q1}-i_{q2} \end{bmatrix}\end{aligned} \tag{8}$$

where R_s is phase resistance, ω_e is rotor angular velocity, u_{d1} and u_{q1} represent dq-axes stator voltage of winding I, i_{d1} and i_{q1} represent dq-axes stator current of winding I, i_{d2} and i_{q2} represent dq-axes stator current of winding II, and ψ_f represents the amplitude of PM flux linkage.

In accordance with (3)-(8), asymmetric mutual-inductances can induce the pulsating impedance in the d-q frame, which can degrade the control performance. During dual-channel operation with identical loads on both windings, where $i_{d1}=i_{d2}$ and $i_{q1}=i_{q2}$, the impact of the asymmetrical mutual-inductance on the voltage equations of one winding set can be canceled out. Conversely, in single-channel operation, the pulsating impedance in the d-q frame caused by asymmetric mutual-inductances can lead to harmonic currents. Specifically, when the stator voltages are sinusoidal, i.e., when u_d and u_q are both dc components, i_d and i_q are the combination of dc components and the negative 2nd-order harmonic components. These harmonics can increase the torque ripple and system losses [14]. Hence, it is critical to minimize current harmonics for working conditions where only one three-phase channel is in operation.

III. Proposed Current Control Scheme

A. SDFT-Based Harmonic Extraction

Generally, DFT can transform the input discrete signals into frequency-domain as

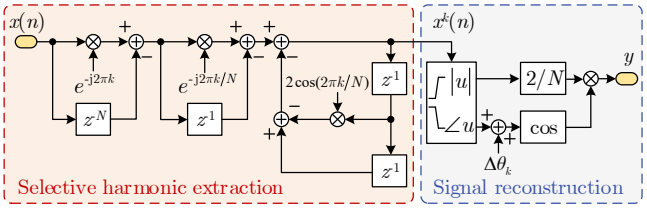

Fig. 4. Block diagram of harmonic detection based on nSDFT.

$$X^k=\sum_{m=0}^{N-1}x(n)W_N^{-mk}\quad k=0,1,\cdots,N-1,\quad W_N=e^{j\frac{2\pi}{N}} \tag{9}$$

where X^k represents the k^{th}-bin frequency component of DFT, $x(n)$ represents the input signal obtained by sampling the time-domain signal $x(t)$ with sampling frequency of f_s, m is the time index, and W_N is the complex twiddle factor. Noted that, direct calculations of the DFT using (9) can impose a high computational burden. Furthermore, during the calculation process, no estimate of the current amplitude of the equivalent sine wave is available. Hence, in recent years, the SDFT which can compute the DFT bins using a recursive scheme was introduced to reduce the computational burden [15]. The difference equation of traditional SDFT can be expressed as

$$X_n^k=\sum_{m=0}^{N-1}x_{q+m}W_N^{-mk}=W_N^k\left(X_{n-1}^k-x_{n-N}+x_n\right) \tag{10}$$

where $q=n$-N+1, X_n^k represents the DFT result for the current window of the sequence $\{x(i),\ i=q,\ q+1,\ q+2,\ldots,\ n\}$, and X_{n-1}^k represents the DFT result for the previous window. That is, the transform window of size N is shifted one sample at a time, repeating the transform process, effectively reducing the computational burden and enabling real-time implementation.

For digital implementation, the discrete z-domain transfer function of SDFT can be expressed as

$$H_{SDFT}(z)=\frac{X^k(z)}{X(z)}=\frac{\left(1-z^{-N}\right)e^{j2\pi k/N}}{1-e^{j2\pi k/N}z^{-1}} \tag{11}$$

Based on (11), several algorithms were proposed to further improve SDFT and ensure the stability. However, in existing methods, the frequency of extracted harmonic should satisfy the following relationship

$$k=\frac{f_{sl}}{\Delta f}=\frac{Nf_{sl}}{f_s} \tag{12}$$

where f_{sl} is the selected frequency to extract, and Δf represents the frequency resolution. Noted that the bin number k usually needs to be integer, which limits the application of the SDFT method in variable-frequency systems such as PMSM drives. To precisely select arbitrary current harmonic in PMSM drive system, a novel non-integer SDFT (nSDFT) [16] from the field of signal processing is employed. This technology has also found application in multi-sampled grid-connected inverters for sideband harmonics suppression [17]. The z-domain transfer function of nSDFT can be expressed as

$$H_{nSDFT}(z)=\frac{e^{-j2\pi k(N-1)/N}-e^{-j2\pi k}z^{-1}-e^{j2\pi k/N}z^{-N}+z^{-N-1}}{1-2\cos(2\pi k/N)z^{-1}+z^{-2}} \tag{13}$$

Then, the arbitrary current harmonic detection based on nSDFT is proposed, with its block diagram shown as Fig. 4. This structure can be seamlessly integrated into the PMSM control scheme and consists of two main parts: selected harmonic extraction and signal reconstruction. Specifically, the specific frequency component of the current can be calculated

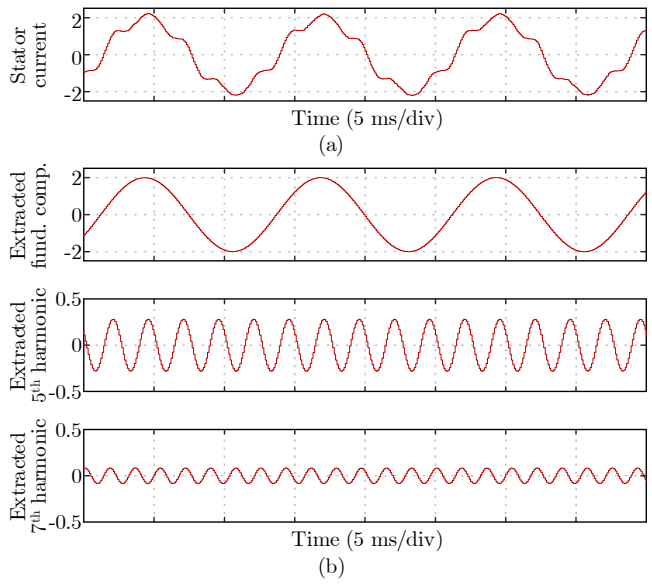

Fig. 5. Verification of nSDFT-based harmonic extraction method. (a) Distorted stator current. (b) Extracted fundamental, 5th, and 7th harmonic components.

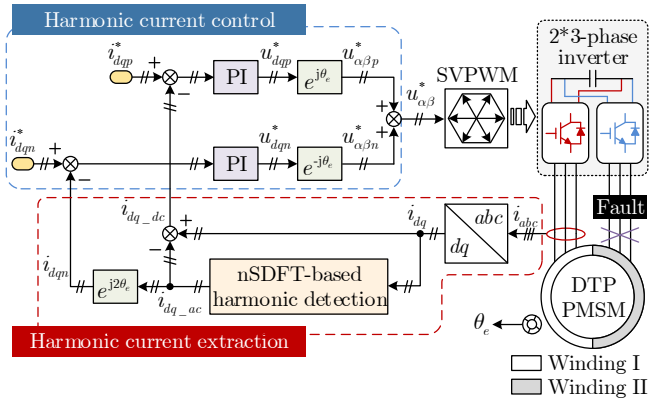

Fig. 6. Block diagram of the proposed current control scheme.

through SDFT and output in complex form, enabling the extraction of both amplitude and phase angle. Moreover, the signal reconstruction on the output complex number can be expressed as

$$y\big|_{k=k_h} = \frac{2}{N}\sqrt{\left\{\mathrm{Re}\left[x(n)H_{nSDFT}(z)\right]\right\}^2 + \left\{\mathrm{Im}\left[x(n)H_{nSDFT}(z)\right]\right\}^2} \cdot\cos\left\{\arctan\frac{\mathrm{Re}\left[x(n)H_{nSDFT}(z)\right]}{\mathrm{Im}\left[x(n)H_{nSDFT}(z)\right]} + \Delta\theta_k\right\} \tag{14}$$

where y is the extracted current harmonic, and $\Delta\theta_k$ is the phase angle correction which equals to $\angle H_{nSDFT}(e^{j2\pi k})$.

A distorted current case is selected to verify the effectiveness of the SDFT-based harmonic extraction algorithm, as illustrated in Fig. 5. The original current is shown in Fig. 5 (a), exhibiting a fundamental frequency of approximately 80 Hz with noticeable distortion. In Fig. 5 (b), the results obtained from three nSDFT-based harmonic extractors, separating the fundamental, 5th, and 7th harmonics at target frequencies of 80, 400, and 560 Hz, are provided. Evidently, the presented harmonic extraction method can effectively extract individual or multiple harmonic components.

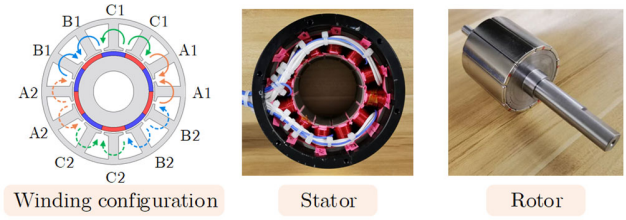

Fig. 7. Down-scaled prototype machine for the experimental verification.

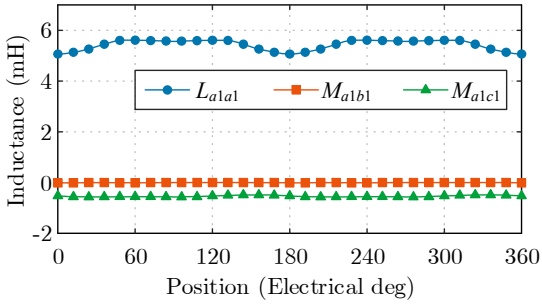

Fig. 8. Inductance waveforms of the down-scaled prototype machine.

B. Overall Control Scheme

Given the analysis above, this part proposes an improved current control scheme that aims to suppress harmonics caused by asymmetric mutual-inductances during single-channel operation mode. The block diagram is depicted in Fig. 5, where subscript *, *p*, and *n* represent the reference, positive-sequence, and negative-sequence component, respectively.

The proposed scheme consists of two parts: a) harmonic current extraction based on nSDFT; and b) harmonic current controller. Due to pulsating impedance, i_{dq} obtained from synchronous coordinate transformation is a combination of dc component and 2nd-order harmonic component. The 2nd-order harmonic current i_{dq_ac} can be obtained by real-time harmonic detection shown as Fig. 4. The dc component i_{dq_dc} of dq-axes currents can be obtained by subtracting i_{dq_ac} from i_{dq}. It is noted that since the proposed harmonic current detection method is based on real-time sliding spectrum analysis, it can accurately extract current harmonics of one or more frequencies without interference from other frequencies. Furthermore, the decomposed current harmonic transformed into negative SRF by the transformation as

$$T_{dq}^{dqn} = \begin{bmatrix} \cos(-2\omega_e t) & \sin(-2\omega_e t) \\ -\sin(-2\omega_e t) & \cos(-2\omega_e t) \end{bmatrix} \tag{15}$$

Based on the proposed harmonic extraction and conversion process, the harmonic currents can be transformed into dc component i_{dqn}. Then, due to the controlled variables in the proposed scheme are all dc components, only the conventional PI controllers are used to regulate the fundamental current and negative-sequence current. This approach implements a current control method using multiple reference frames. The bandwidth of the PI controllers in each reference frame should not exceed that of the harmonic component detection to ensure accurate regulation of harmonic currents to their reference values [18]. The negative-sequence current caused by asymmetric mutual-inductances can be suppressed by setting the references to zero. The input of the modulation strategy, i.e., the reference voltage, consists of the sum of positive-sequence output voltages $u_{\alpha\beta p}^*$ and negative-sequence output voltages $u_{\alpha\beta n}^*$. In the

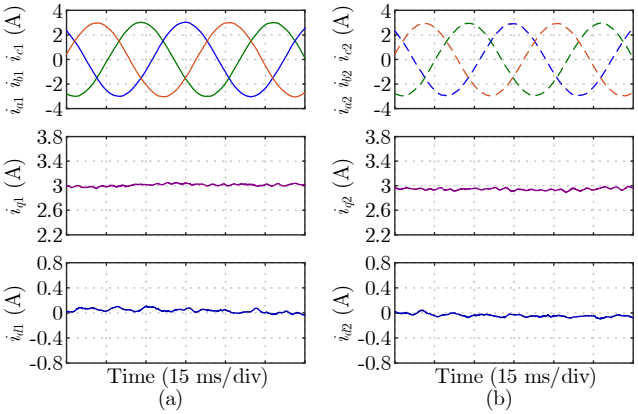

Fig. 9. Experimental results of two-channel operation mode. (a) Winding I. (b) Winding II.

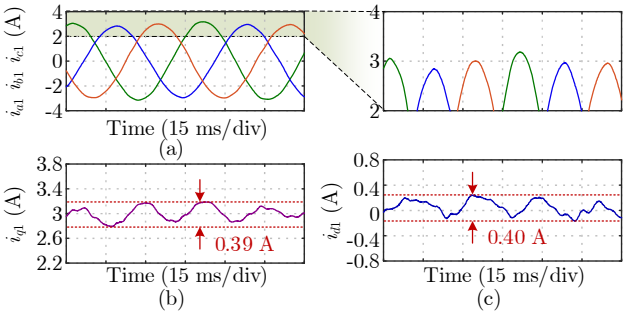

Fig. 10. Experimental results of single-channel operation mode. (a) Phase currents. (b) q-axis current. (c) d-axis current.

proposed scheme, only simple PI regulators are used, thus avoiding complex controller design and excessive parameter tuning.

IV. Experimental Verification

The proposed control method is experimentally validated on a down-scaled DTP PMSM as depicted in Fig. 7. An internal-rotor prototype machine with zero angle displacement is manufactured, with each set of three-phase windings distributed in half of the stator as shown in Fig. 2. The inductance waveforms of this machine are presented in Fig. 8, revealing noticeable mutual-inductance asymmetry. The test machine is driven by two three-phase inverters and digitally controlled within a dSPACE system. The sampling frequency is set to be the same as the switching frequency, which is 10 kHz.

Fig. 9 shows the experimental results of the two-channel operation. The reference speed is set as 240 r/min. Due to the coupling effect between the two sets of windings, the three-phase currents of each winding are symmetric and there are no obvious harmonics in dq-axis currents. As a comparison, Fig. 10 presents experimental results of single-channel operation mode. It is noticeable that three-phase currents are unbalanced, and there exist 2nd-order harmonics in dq-axis currents, which can degrade the system performance. This implies that even for a well-designed DTP PMSM with zero angle displacement, unbalanced currents will also exist under single-channel operation, aligning with the presented theoretical analysis.

Fig. 11 displays experimental results of the single-channel operation mode with the proposed control method. The

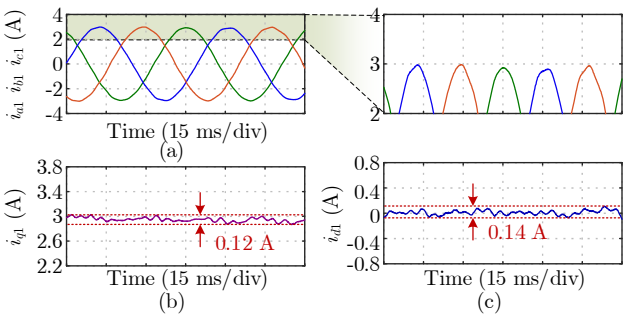

Fig. 11. Experimental results of one channel operation mode with proposed control method. (a) Phase currents. (b) q-axis current. (c) d-axis current.

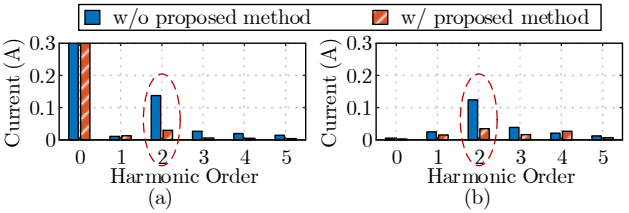

Fig. 12. Harmonic spectrum comparison. (a) q-axis current. (b) d-axis current.

fluctuations in q- and d-axis current decrease from 0.39 A and 0.40 A to 0.12 A and 0.14 A, respectively, indicating that the proposed method has a decent harmonic suppression effect. Moreover, Fig. 12 illustrates a comparison of the harmonic spectrum with and without the proposed method. It is evident that the 2nd-order harmonics caused by asymmetric mutual-inductances can be effectively attenuated through the utilization of the proposed method.

V. Conclusion

This letter concentrates on the issue of current harmonics in symmetrical DTP PMSMs, with a specific emphasis on the single-channel operation mode. The research shows that the asymmetric mutual-inductances caused by asymmetric relative position between one set of windings can contribute to negative-sequence currents, a phenomenon that is particularly evident in single-channel operation. In response, a flexible harmonic control method utilizing nSDFT is proposed to mitigate these undesired harmonics. The achievements are outlined below.

1) Only conventional PI controllers are used, eliminating the need for additional parameter tuning or digital filters.
2) The frequency of target harmonic can be flexibly selected, allowing the proposed scheme to be applied for arbitrary current harmonic detection and regulation.

Finally, the effectiveness of the presented analysis and proposed method is verified by laboratory tests. These tests confirm the existence of negative sequence current, and demonstrate that the proposed scheme effectively suppresses dq-axis harmonic current ripples.

References

[1] E. Levi, "Multiphase electric machines for variable-speed applications," *IEEE Trans. Ind. Electron*., vol. 55, no. 5, pp. 1893-1909, May. 2008.

[2] Z. Xue, S. Niu, A. M. H. Chau, Y. Luo, H. Lin, and X. Li, "Recent advances in multi-phase electric drives model predictive control in renewable energy application: A state-of-the-art review," *World Electric Veh. J.*, vol. 14, no. 2, 2023, Art. no. 44.

[3] Z. Q. Zhu, S. Wang, B. Shao, L. Yan, P. Xu, and Y. Ren, “Advances in dual-three-phase permanent magnet synchronous machines and control techniques,” *Energies*, vol. 14, no. 22, Nov. 2021, Art. no. 7508.

[4] G. Feng, Y. Lu, C. Lai, B. Ding and N. C. Kar, "Fault tolerant maximum torque per ampere (FT-MTPA) control for dual three-phase interior PMSMs under open-phase fault," *IEEE Trans. Ind. Electron*., vol. 69, no. 12, pp. 12030-12041, Dec. 2022.

[5] Y. Luo and S. Niu, "Predictive current control for six-phase PMSM motor with multi-step synthesis based virtual vectors," *IEEE Trans. Energy Convers*., vol. 38, no. 1, pp. 134-146, Mar. 2023.

[6] Y. Zhao and T. A. Lipo, “Space vector PWM control of dual three-phase induction machine using vector space decomposition,” *IEEE Trans. Ind. Appl.*, vol. 31, no. 5, pp. 1100–1109, Sep. 1995.

[7] Y. Hu, Z. Q. Zhu, and K. Liu, “Current control for dual three-phase permanent magnet synchronous motors accounting for current unbalance and harmonics,” *IEEE J. Emerg. Select. Top. Power Electron.*, vol. 2, no. 2, pp. 272–284, Jun. 2014.

[8] J. Karttunen, S. Kallio, J. Honkanen, P. Peltoniemi and P. Silventoinen, "Partial current harmonic compensation in dual three-phase PMSMs considering the limited available voltage," *IEEE Trans. Ind. Electron*., vol. 64, no. 2, pp. 1038-1048, Feb. 2017.

[9] Y. Du, L. Wu, Z. Lyu, Y. Fang, X. Wu and Q. Lyu, "Influence of start rotor position on three-phase short-circuit current in dual three-phase surface-mounted PM machines," *IEEE Trans. Ind. Electron*., vol. 69, no. 5, pp. 4419-4430, May. 2022.

[10] M. Barcaro, N. Bianchi, and F. Magnussen, “Analysis and tests of a dual three-phase 12-slot 10-pole permanent-magnet motor,” *IEEE Trans. Ind. Appl.*, vol. 46, no. 6, pp. 2355–2362, Nov./Dec. 2010.

[11] P. Catalán, Y. Wang, J. Arza and Z. Chen, "A comprehensive overview of power converter applied in high-power wind turbine: key challenges and potential solutions," *IEEE Trans. Power Electron.*, vol. 38, no. 5, pp. 6169-6195, May. 2023.

[12] J. A. Swanke and T. M. Jahns, "Reliability analysis of a fault-tolerant integrated modular motor drive for an urban air mobility aircraft using Markov chains," *IEEE Trans. Transport. Electrific.*, vol. 8, no. 4, pp. 4523-4533, Dec. 2022.

[13] Z. Li, L. Wu, Z. Chen, Y. Shi, L. Qiu and Y. Fang, "Single- and two-phase open-circuit fault tolerant control for dual three-phase PM motor without phase shifting," *IEEE Access*, vol. 8, pp. 171945-171955, 2020.

[14] Z. Lyu, S. Niu, M. Hu, *et al*., "Improving dc-link voltage utilization in PMSM drives with resistance asymmetry via active harmonic injection," *IEEE Trans. Transp. Electrific.*, early access.

[15] C. -S. Park, "Fast, accurate, and guaranteed stable sliding discrete Fourier transform [sp Tips&Tricks]," *IEEE Signal Process. Mag.*, vol. 32, no. 4, pp. 145-156, Jul. 2015.

[16] R. Lyons and C. Howard, "Improvements to the sliding discrete Fourier transform algorithm [Tips & Tricks]," *IEEE Signal Process. Mag.*, vol. 38, no. 4, pp. 119-127, Jul. 2021.

[17] T. Wang, W. Yao, H. Yang, W. Li and Z. Ou, "Dissipativity enhancement for multisampled LCL-type inverter using a low-delay ripple-removal method," *IEEE J. Emerg. Sel. Topics Power Electron.*, vol. 11, no. 5, pp. 4784-4798, Oct. 2023.

[18] G. Feng, C. Lai, J. Tian and N. C. Kar, "Multiple reference frame based torque ripple minimization for PMSM drive under both steady-state and transient conditions," *IEEE Trans. Power Electron.*, vol. 34, no. 7, pp. 6685-6696, July 2019.